How to interpret the spectral density of the Keldysh nonequilibrium Green's function

K.J. Pototzky and E.K.U. Gross
Max Planck Institute of Microstructure Physics, 06120 Halle (Saale), Germany
(Dated: February 25, 2022)

This paper is devoted to the study and interpretation of the spectral function $\mathbf{A}(\omega, T)$ of the Keldysh nonequilibrium Green's function. The spatial diagonal of the spectral function is often interpreted as a time-dependent local density of states. We show that this object can take negative values implying that a simple probability interpretation as a time-dependent density of states is not possible. The same issue also occurs for the Wigner function $P(x, p)$ where it is solved by taking the uncertainty principle into account. We follow the same path and incorporate the time-energy uncertainty relation to define a convoluted spectral function that allows for a probability interpretation. The usefulness of this quantity as a interpretative tool is demonstrated by visualizing the charge dynamics in a quantum dot coupled to superconducting leads.

PACS numbers: 73.63.-b 74.40.Gh 85.25.Cp 73.63.Kv

I. INTRODUCTION

The ongoing miniaturization of electronics may ultimately lead to the use of single molecules as its building blocks. A sound theoretical understanding of phenomena in nanojunctions is therefore of great importance. Since the first proposal of using a molecule as an electronic component by Aviram and Ratner in 1974,[1] an enormous number of research articles have appeared. Several textbooks, e.g. Refs 2–4, serve as excellent introductions to the field.

While, traditionally, the prime quantity of interest was the current-voltage characteristics of the molecular junction, calculated or measured in the steady state, there has been a shift of attention towards time-resolved studies of quantum transport in recent years.[5–9] With this type of studies one may address questions like: How much time does it take until the steady state is reached and, by which structural changes in the junction, can this switching time be made shorter or longer? Is there a steady state at all? If there is a steady state, is it unique? If it is not unique, how can one switch between multiple steady states? On the theoretical side, various approaches have been put forth to study the real-time dynamics of molecular junctions. Among those are the Kadanoff-Baym equations[5,6,10,11] representing the time-dependent variety of many-body perturbation theory, time-dependent density functional theory,[12–19] the time-dependent tight binding approach,[20–22] the hierachy equation of motion approach,[23–25] the multi-configuration time-dependent Hartree-Fock method[26–29] as well as Quantum Monte-Carlo.[30]

Once the numerical time propagation of the respective equation of motion has been performed, the next question is about the tools to interpret and visualize the results. One possibility is the time-dependent electron localization function,[31,32] a correlation function suitable to visualize chemical bonds.

In this article we investigate another quantity, the spectral function $\mathbf{A}(\omega, T)$ of the Keldysh non-equilibrium Green's function. This object is more targeted towards the understanding of charger-transfer processes and has provided valuable insights in the internal dynamics of molecular junctions.[5–9] The definition of the spectral functions[10] is

$$\mathbf{A}(\omega, T) = \int_{-\infty}^{\infty} \frac{d\tau}{2\pi} e^{i\omega\tau} \mathbf{A}\left(T + \frac{\tau}{2}, T - \frac{\tau}{2}\right), \quad (1)$$

$$\mathbf{A}(t, t') = i\left[\mathbf{G}^{>}(t, t') - \mathbf{G}^{<}(t, t')\right] \quad (2)$$

where $\mathbf{G}^{\gtrless}(t, t')$ are the standard greater (lesser) nonequilibrium Green's functions.[10] $\mathbf{A}(\omega, T)$ is a matrix with respect to some representation referring, e.g., to space and spin coordinates $\mathbf{A}_{r\sigma,r'\sigma'}(\omega, T)$ or to localized orbitals $\mathbf{A}_{i,j}(\omega, T)$. The objective of this article is to give a clear-cut physical interpretation of the diagonal of this matrix. In particular we shall investigate whether and to which extend it can be viewed as a time-dependent density of states.

The paper is structured as follows: In the next section, we explain the model of a quantum dot coupled to superconducting leads, state the corresponding Hamiltonian and define all necessary nonequilibrium Green's functions. In section III we derive a method to calculate the large-time behaviour of $\mathbf{A}(\omega, T)$ directly from the defining equations. We further present a second method using single particle wave functions which give access to $\mathbf{A}(\omega, T)$ at all times T. This, in particular, allows the visualization of switching effects. In section IV, we show with a simple example that the probability interpretation of the spectral function is generally not correct because it can take negative values. We solve this problem by taking the time-energy uncertainty relation into account. In section V, we study the spectral function in two situations with a change in the bias. First, we switch on the bias in a step-like fashion and look at the spectral function decomposed into contributions of scattering and bound states. Second, we visualize the spectral function of the Andreev bound states under the influence of a rectangular bias pulse. The final section VI summarizes the outcome of the presented work.

II. THEORETICAL FOUNDATION

A. The Model

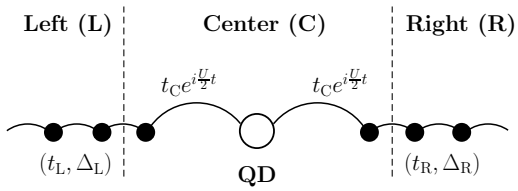

FIG. 1. A sketch of the tight binding model. The filled dots represent the sites of the superconducting leads while the central site (the quantum dot) is normal conducting. The left and right site of the central region are buffer sites of the leads.

The model is a tight binding chain of atoms where the central region consists of a quantum dot (QD) and two buffer sites of the leads, one in each direction. A sketch is shown in figure 1. The sites are enumerated from left to right with 0 being the quantum dot (QD). Filled dots represent superconducting sites, the empty one is normal-conducting.

The bias enters the model Hamiltonian using Peierls' substitution.[33] The Hamiltonian reads as

$$\hat{H} = \hat{H}_{\text{Center}}(t) + \hat{H}_{\text{tunnelling}} + \hat{H}_{\text{Leads}} \tag{3}$$

$$\begin{aligned}\hat{H}_{\text{Center}}(t) = &\sum_{\sigma\in\{\uparrow,\downarrow\}} \left(t_C e^{i\frac{U}{2}t}\hat{c}^\dagger_{-1,\sigma}\hat{c}_{\text{QD},\sigma} + H.c.\right) \\ &+ \sum_{\sigma\in\{\uparrow,\downarrow\}} \left(t_C e^{i\frac{U}{2}t}\hat{c}^\dagger_{\text{QD},\sigma}\hat{c}_{1,\sigma} + H.c.\right) \\ &+ \left(\Delta_L \hat{c}^\dagger_{-1,\uparrow}\hat{c}^\dagger_{-1,\downarrow} + H.c.\right) \\ &+ \left(\Delta_R \hat{c}^\dagger_{1,\uparrow}\hat{c}^\dagger_{1,\downarrow} + H.c.\right),\end{aligned} \tag{4}$$

$$\begin{aligned}\hat{H}_{\text{tunnelling}} = &\sum_{\sigma\in\{\uparrow,\downarrow\}} \left(t_L \hat{c}^\dagger_{-2,\sigma}\hat{c}_{-1,\sigma} + H.c.\right) \\ &+ \sum_{\sigma\in\{\uparrow,\downarrow\}} \left(t_R \hat{c}^\dagger_{1,\sigma}\hat{c}_{2,\sigma} + H.c.\right),\end{aligned} \tag{5}$$

$$\begin{aligned}\hat{H}_{\text{Leads}} = &\sum_{k=-\infty}^{-2} \left(\Delta_L \hat{c}^\dagger_{k,\uparrow}\hat{c}^\dagger_{k,\downarrow} + H.c.\right) \\ &+ \sum_{k=-\infty}^{-2}\sum_{\sigma\in\{\uparrow,\downarrow\}} \left(t_L \hat{c}^\dagger_{k-1,\sigma}\hat{c}_{-k,\sigma} + H.c.\right) \\ &+ \sum_{k=2}^{\infty} \left(\Delta_R \hat{c}^\dagger_{k,\uparrow}\hat{c}^\dagger_{k,\downarrow} + H.c.\right) \\ &+ \sum_{k=2}^{\infty}\sum_{\sigma\in\{\uparrow,\downarrow\}} \left(t_R \hat{c}^\dagger_{k,\sigma}\hat{c}_{k+1,\sigma} + H.c.\right).\end{aligned} \tag{6}$$

All parameters of the model Hamiltonian are chosen real valued and positive. We use symmetric leads throughout this article, i.e. $\Delta_L = \Delta_R = \Delta$ and $t_L = t_R = t$. Furthermore, we will work in the wide-band limit which corresponds to $t_\alpha \gg t_C$. Hence the results do not depend on t_α and t_C independently, but only on the coupling $\Gamma_\alpha = \frac{2t_C^2}{t_\alpha}$. We point out that one has to solve the time-dependent Bogoliubov de-Gennes equation, which is a Schrödinger-like equation in the electron-hole space. The corresponding matrices in electron-hole basis are written in bold-face letters.

It is useful to follow the convention introduced by Yoichiro Nambu[34] and group the operators in two dimensional vectors:

$$\hat{\psi}^\dagger_k = \begin{pmatrix}\hat{c}^\dagger_{k,\uparrow} & \hat{c}_{k,\downarrow}\end{pmatrix}, \qquad \hat{\psi}_k = \begin{pmatrix}\hat{c}_{k,\uparrow} \\ \hat{c}^\dagger_{k,\downarrow}\end{pmatrix}. \tag{7}$$

The upper component represents spin up electrons, the lower component can be interpreted as spin down holes.

For later use, it is convenient to define projections of $\mathbf{H}$, which is the matrix representation of the Hamiltonian $\hat{H}$ in Nambu space, onto the different subspaces. In terms of these projections, the full Hamiltonian $\mathbf{H}(t)$ can be partitioned as

$$\mathbf{H}(t) = \begin{pmatrix}\mathbf{H}_{\text{LL}} & \mathbf{H}_{\text{LC}} & 0 \\ \mathbf{H}_{\text{CL}} & \mathbf{H}_{\text{CC}}(t) & \mathbf{H}_{\text{CR}} \\ 0 & \mathbf{H}_{\text{RC}} & \mathbf{H}_{\text{RR}}\end{pmatrix}. \tag{8}$$

On the other hand, the matrix $\mathbf{H}_{\text{CC}}(t)$ can be partitioned as

$$\mathbf{H}_{\text{CC}}(t) = \begin{pmatrix}\mathbf{H}_{-1,-1} & \mathbf{H}_{-1,\text{QD}}(t) & 0 \\ \mathbf{H}_{\text{QD},-1}(t) & \mathbf{H}_{\text{QD}} & \mathbf{H}_{\text{QD},1}(t) \\ 0 & \mathbf{H}_{1,\text{QD}}(t) & \mathbf{H}_{1,1}\end{pmatrix}. \tag{9}$$

B. Definition of the nonequilibrium Green's function

In the following sections we will make use of the Keldysh nonequilibrium Green's functions (NEGF). We shall define all necessary objects. For details, we refer the reader to the book by Stefanucci and van Leeuwen[10] for an excellent comprehensive introduction to nonequilibrium Green's functions. The usual Keldysh contour γ is sketched in figure 2.

The nonequilibrium Green's function is defined as

$$\mathbf{G}(z,z') = -i\langle \mathcal{T}_C \hat{\psi}_{\text{H}}(z)\hat{\psi}^\dagger_{\text{H}}(z')\rangle \tag{10}$$

$$= \Theta(z,z')\mathbf{G}^>(z,z') + \Theta(z',z)\mathbf{G}^<(z,z') \tag{11}$$

with the time-contour ordering operator $\mathcal{T}_C$ and the field operators $\hat{\psi}_{\text{H}}(z)$ and $\hat{\psi}^\dagger_{\text{H}}(z)$ in the Heisenberg picture. The lesser and greater Green's functions for real time arguments are given by

$$\mathbf{G}^<(t,t') = i\langle \hat{\psi}^\dagger_{\text{H}}(t')\hat{\psi}_{\text{H}}(t)\rangle, \tag{12}$$

$$\mathbf{G}^>(t,t') = -i\langle \hat{\psi}_{\text{H}}(t)\hat{\psi}^\dagger_{\text{H}}(t')\rangle. \tag{13}$$

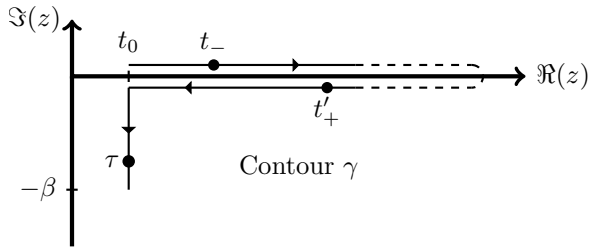

FIG. 2. Sketch of the Keldysh contour γ in the complex time plane. Variables $t_\pm$ denote times on the upper $(-)$ or lower $(+)$ branch of the horizontal part. The variable τ is used for times on the vertical part.

The nonequilibrium Green's functions can be partitioned in the same way as the Hamiltonian:

$$\mathbf{G}^{\gtrless}(z,z') = \begin{pmatrix} \mathbf{G}^{\gtrless}_{\mathrm{LL}}(z,z') & \mathbf{G}^{\gtrless}_{\mathrm{LC}}(z,z') & \mathbf{G}^{\gtrless}_{\mathrm{LR}}(z,z') \\ \mathbf{G}^{\gtrless}_{\mathrm{CL}}(z,z') & \mathbf{G}^{\gtrless}_{\mathrm{CC}}(z,z') & \mathbf{G}^{\gtrless}_{\mathrm{CR}}(z,z') \\ \mathbf{G}^{\gtrless}_{\mathrm{RL}}(z,z') & \mathbf{G}^{\gtrless}_{\mathrm{RC}}(z,z') & \mathbf{G}^{\gtrless}_{\mathrm{RR}}(z,z') \end{pmatrix}. \tag{14}$$

The same can be done for the spectral function $\mathbf{A}(t,t')$. Similar to the partitioning of $\mathbf{H}_{\mathrm{CC}}(t)$ in equation (9), we will use $\mathbf{G}^{\gtrless}_{\mathrm{QD}}(z,z')$ and $\mathbf{A}_{\mathrm{QD}}(t,t')$ in the course of this work to denote the central entry of $\mathbf{G}^{\gtrless}_{\mathrm{CC}}(z,z')$ and $\mathbf{A}_{\mathrm{CC}}(t,t')$.

III. CALCULATING THE SPECTRAL FUNCTION

A. NEGF based method

We want to calculate the large time behaviour of the spectral function $\mathbf{A}_{\mathrm{CC}}(\omega,T)$ with respect to T. We point out that the limit $\lim_{T\to\infty}\mathbf{A}_{\mathrm{CC}}(\omega,T)$ in general does not exist, i.e. $\mathbf{A}_{\mathrm{CC}}(\omega,T)$ is a nontrivial function of T even for large T. We are specifically interested in this T-dependence of $\mathbf{A}_{\mathrm{CC}}(\omega,T)$ for large times, i.e. we dot not study transient effects. We start from the definition of the spectral function $\mathbf{A}(t,t')$ given in section I:

$$\mathbf{A}(t,t') = i\left[\mathbf{G}^{>}(t,t') - \mathbf{G}^{<}(t,t')\right]. \tag{15}$$

Next we use reformulate the Green's functions $\mathbf{G}^{\gtrless}_{\mathrm{CC}}(t,t')$ in a way similar to Refs 35 and 36, by using the embedding self-energy

$$\mathbf{\Sigma}_\alpha(z,z') = \mathbf{H}_{\mathrm{C}\alpha}\mathbf{g}_{\alpha\alpha}(z,z')\mathbf{H}_{\alpha\mathrm{C}}, \tag{16}$$

where $\mathbf{g}_{\alpha\alpha}(z,z')$ is the nonequilibrium Green's function of the isolated lead α. We finally arrive at:

$$\begin{aligned}
&\mathbf{G}^{\gtrless}_{\mathrm{CC}}(t,t') \qquad (17)\\
&= \sum_{\alpha,\alpha'\in\{\mathrm{L,C,R}\}} \mathbf{G}^{\mathrm{R}}_{\mathrm{C}\alpha}(t,t_0)\mathbf{G}^{\gtrless}_{\alpha\alpha'}(t_0,t_0)\mathbf{G}^{\mathrm{A}}_{\alpha'\mathrm{C}}(t_0,t') \\
&= \mathbf{G}^{\mathrm{R}}_{\mathrm{CC}}(t,t_0)\mathbf{G}^{\gtrless}_{\mathrm{CC}}(t_0,t_0)\mathbf{G}^{\mathrm{A}}_{\mathrm{CC}}(t_0,t') \qquad (18)\\
&\quad - i\sum_{\alpha\in\{\mathrm{L,R}\}} [\mathbf{G}^{\mathrm{R}}_{\mathrm{CC}}\cdot\mathbf{\Sigma}^{\rceil}_\alpha \star \mathbf{G}^{\lceil}_{\mathrm{CC}}](t,t_0)\mathbf{G}^{\mathrm{A}}_{\mathrm{CC}}(t_0,t') \\
&\quad + \sum_{\alpha\in\{\mathrm{L,R}\}} \mathbf{G}^{\mathrm{R}}_{\mathrm{CC}}(t,t_0)[\mathbf{G}^{\rceil}_{\mathrm{CC}} \star \mathbf{\Sigma}^{\lceil}_\alpha\cdot\mathbf{G}^{\mathrm{A}}_{\mathrm{CC}}](t_0,t') \\
&\quad + \sum_{\alpha\in\{\mathrm{L,R}\}} [\mathbf{G}^{\mathrm{R}}_{\mathrm{CC}}\cdot\mathbf{\Sigma}^{\gtrless}_\alpha\cdot\mathbf{G}^{\mathrm{A}}_{\mathrm{CC}}](t,t') \\
&\quad + \sum_{\alpha,\alpha'\in\{\mathrm{L,R}\}} [\mathbf{G}^{\mathrm{R}}_{\mathrm{CC}}\cdot\mathbf{\Sigma}^{\rceil}_\alpha \star \mathbf{G}^{\mathrm{M}}_{\mathrm{CC}} \star \mathbf{\Sigma}^{\lceil}_{\alpha'}\cdot\mathbf{G}^{\mathrm{A}}_{\mathrm{CC}}](t,t').
\end{aligned}$$

The superscripts $\lceil$ ($\rceil$, M) indicate that the first (second, both) time argument lies on the vertical part of the Keldysh contour. We further have employed the notation

$$[\boldsymbol{A}\cdot\boldsymbol{B}](t,t') = \int_{t_0}^{\infty} d\bar{t}\,\boldsymbol{A}(t,\bar{t})\boldsymbol{B}(\bar{t},t'), \tag{19}$$

$$[\boldsymbol{A}\star\boldsymbol{B}](t,t') = \int_{t_0}^{t_0-i\beta} d\tau\,\boldsymbol{A}(t,\tau)\boldsymbol{B}(\tau,t'). \tag{20}$$

Multiple products are defined analogously, i.e. $[\boldsymbol{A}\cdot\boldsymbol{B}\cdot\boldsymbol{C}](t,t') = [\boldsymbol{A}\cdot[\boldsymbol{B}\cdot\boldsymbol{C}]](t,t')$. To investigate the large-time behaviour of $\mathbf{G}^{\gtrless}_{\mathrm{CC}}(t,t')$ with both time arguments being large, we set $t,t' > b$ and take the limit $b\to\infty$. We choose the initial system at t_0 such that it does not have any bound states and so that we can assume

$$\lim_{t\to\infty}\mathbf{G}_{\mathrm{CC}}(t_\pm,z') = \lim_{t'\to\infty}\mathbf{G}_{\mathrm{CC}}(z,t'_\pm) = 0, \tag{21}$$

$$\lim_{t\to\infty}\mathbf{\Sigma}_\alpha(t_\pm,z') = \lim_{t'\to\infty}\mathbf{\Sigma}_\alpha(z,t'_\pm) = 0 \tag{22}$$

for fixed z,z' on the Keldysh contour. We can now drop all terms in equation (18) that tend to zero as $b\to\infty$ and finally arrive at:

$$\mathbf{G}^{\gtrless}_{\mathrm{CC}}(t,t') \overset{t,t'\to\infty}{\sim} \left[\mathbf{G}^{\mathrm{R}}_{\mathrm{CC}}\cdot\mathbf{\Sigma}^{\gtrless}\cdot\mathbf{G}^{\mathrm{A}}_{\mathrm{CC}}\right](t,t'). \tag{23}$$

We use the symbol $\sim$ to denote the norm convergence, i.e. $X(t,t') \overset{t,t'\to\infty}{\sim} Y(t,t')$ means $\lim_{t,t'\to\infty}\|X(t,t') - Y(t,t')\| = 0$. The next step consists in specifying the Hamiltonian. According to the definition of the central Hamiltonian in equation (9), we can write it as

$$\mathbf{H}_{\mathrm{CC}}(t) = \mathbf{H}^0_{\mathrm{CC}} + \mathbf{U}_+ e^{i\omega_0 t} + \mathbf{U}_- e^{-i\omega_0 t} \tag{24}$$

with $\omega_0 = \frac{U}{2}$. We now assume that our system with the applied bias does not have any bound states and that the T-dependence of all observables is periodic with frequency ω_0. As opposed to the work of Ref 36, our system

has a minor history and initial state dependence, which only shows up in a phase shift of the periodic observables. As we will later set the initial time t_0 to $-\infty$, this phase is by design not accessible. This allows us to represent the advanced and retarded Green's function of the central region as[36]

$$\begin{aligned}\mathbf{G}^{\mathrm{R,A}}_{\mathrm{CC}}(t,t') &= \sum_{m\in\mathbb{Z}}\int_{-\infty}^{\infty}\frac{d\omega}{2\pi}\widetilde{\mathbf{G}}^{\mathrm{R,A}}_{m}(\omega)e^{-i\omega(t-t')+im\omega_0\frac{t+t'}{2}}\\ &= \sum_{m\in\mathbb{Z}}\int_{-\infty}^{\infty}\frac{d\omega}{2\pi}\mathbf{G}^{\mathrm{R,A}}_{m}(\omega)e^{-i\omega(t-t')+im\omega_0 t'}.\end{aligned} \tag{25}$$

The equivalence of the two expansions can be easily checked by a variable substitution in the integral. We use the latter representation for convenience reasons.

The embedding self-energies $\mathbf{\Sigma}^{\mathrm{R,A,}\gtrless}_{\alpha}(t,t')$ depend only on the time difference $t-t'$, thus we can write $\mathbf{\Sigma}^{\mathrm{R,A,}\gtrless}_{\alpha}(t-t')$ in terms of its Fourier transform:

$$\mathbf{\Sigma}^{\mathrm{R,A,}\gtrless}_{\alpha}(t-t') = \int_{-\infty}^{\infty}\frac{d\omega}{2\pi}e^{-i\omega(t-t')}\mathbf{\Sigma}^{\mathrm{R,A,}\gtrless}_{\alpha}(\omega). \tag{26}$$

At this point, it is convenient to set the initial time t_0 of the Keldysh contour to $-\infty$. We insert the expansions (25) and (26) into equation (23) and carry out the integrals, leading to the final expression

$$\begin{aligned}\mathbf{A}_{\mathrm{CC}}(\omega,T) \overset{T\to\infty}{\sim} \frac{1}{2\pi}\sum_{\boldsymbol{m}\in\mathbb{Z}^2} e^{i(m_1+m_2)\omega_0 T} \\ \cdot\,\mathbf{G}_{m_1}\left(\omega+\frac{\omega_0}{2}(m_1-m_2)\right)\\ \cdot\,\mathbf{\Gamma}\left(\omega+\frac{\omega_0}{2}(m_1-m_2)\right)\\ \cdot\,\mathbf{G}^{\dagger}_{-m_2}\left(\omega+\frac{\omega_0}{2}(m_1-m_2)\right),\end{aligned} \tag{27}$$

$$\mathbf{A}_{\mathrm{CC,DC}}(\omega) = \lim_{\tilde{t}\to\infty}\frac{\omega_0}{2\pi}\int_{\tilde{t}}^{\tilde{t}+\frac{2\pi}{\omega_0}} dT\,\mathbf{A}_{\mathrm{CC}}(\omega,T) \tag{28}$$

$$\begin{aligned}&= \frac{1}{2\pi}\sum_{m\in\mathbb{Z}}\mathbf{G}_m(\omega+\omega_0 m) \\ &\quad \mathbf{\Gamma}(\omega+\omega_0 m)\,\mathbf{G}^{\dagger}_m(\omega+\omega_0 m),\end{aligned} \tag{29}$$

with

$$\mathbf{\Gamma}_{\alpha}(\omega) = i\left[\mathbf{\Sigma}^{\mathrm{R}}_{\alpha}(\omega)-\mathbf{\Sigma}^{\mathrm{A}}_{\alpha}(\omega)\right], \tag{30}$$

$$\mathbf{\Gamma}(\omega) = \mathbf{\Gamma}_{\mathrm{L}}(\omega)+\mathbf{\Gamma}_{\mathrm{R}}(\omega), \tag{31}$$

$$\mathbf{G}_m(\omega) = \mathbf{G}^{\mathrm{R}}_m(\omega-m\omega_0) = \left[\mathbf{G}^{\mathrm{A}}_{-m}(\omega)\right]^{\dagger}. \tag{32}$$

The matrices $\mathbf{G}_m(\omega)$ are calculated by using a scheme proposed by Stefanucci *et al.*.[36]

The analytic expression for the embedding self-energies $\mathbf{\Sigma}^{\mathrm{R/A}}_{\alpha}(\omega)$ of our model Hamiltonian reads:[37]

$$\mathbf{\Sigma}^{\mathrm{R/A}}_{\alpha}(\omega) = \lim_{\eta\searrow 0}\begin{pmatrix}\tilde{m}_{\alpha}(\omega\pm i\eta) & \tilde{d}_{\alpha}(\omega\pm i\eta)\\ \tilde{d}_{\alpha}(\omega\pm i\eta) & \tilde{m}_{\alpha}(\omega\pm i\eta)\end{pmatrix}, \tag{33}$$

$$\tilde{m}_{\alpha}(z) = \frac{z}{2}\frac{\sqrt{\Delta_{\alpha}^2-z^2}-\sqrt{\Delta_{\alpha}^2-z^2+4t_{\alpha}^2}}{\sqrt{\Delta_{\alpha}^2-z^2}}, \tag{34}$$

$$\tilde{d}_{\alpha}(z) = \frac{\Delta_{\alpha}}{2}\frac{\sqrt{z^2-\Delta_{\alpha}^2-4t_{\alpha}^2}-\sqrt{z^2-\Delta_{\alpha}^2}}{\sqrt{z^2-\Delta_{\alpha}^2}}. \tag{35}$$

In the numerical implementation, one has to use a finite value of η which will be stated in the results for the sake of completeness.

The remaining problem is the numerical evaluation of the infinite sum in equation (27). We do this by truncation at some large value $m_{\max}$ i.e. the sum runs over $\|\boldsymbol{m}\| < m_{\max}, \boldsymbol{m}\in\mathbb{Z}^2$. Of course, the convergence of the results with respect to $m_{\max}$ has to be checked carefully.

B. Time propagation method

An alternative way to calculate the nonequilibrium Green's functions $\mathbf{G}^{\gtrless}(t,t')$ is to use propagated single particle wave functions $\psi_q(t) = (u_q(t), v_q(t))^T$.

We start in the ground state at $t=0$ and carry out a time propagation only in the central region, i.e. we solve

$$\begin{aligned}[i\partial_t - \mathbf{H}_{\mathrm{CC}}(t)]\psi_{q,\mathrm{C}}(t) = \\ \sum_{\alpha\in\{\mathrm{L,R}\}}\int_0^t dt'\mathbf{\Sigma}^{\mathrm{R}}_{\alpha}(t,t')\psi_{q,\mathrm{C}}(t')\\ + \sum_{\alpha\in\{\mathrm{L,R}\}}\mathbf{H}_{\mathrm{C}\alpha}\mathbf{g}^{\mathrm{R}}_{\alpha\alpha}(t,0)\psi_{q,\alpha}(0).\end{aligned} \tag{36}$$

We refer the reader to the work of Stefanucci *et al.*[38] for details of the propagation scheme.

Having the single particle wave functions $\psi_q(t)$ at hand, we can calculate the spectral function $\mathbf{A}(t,t')$ as

$$[\mathbf{A}(t,t')]_{kl} = \sum\!\!\!\!\!\!\int_q \begin{pmatrix}u_{q,k}(t)\,[u_{q,l}(t')]^{\star} & u_{q,k}(t)\,[v_{q,l}(t')]^{\star}\\ v_{q,k}(t)\,[u_{q,l}(t')]^{\star} & v_{q,k}(t)\,[v_{q,l}(t')]^{\star}\end{pmatrix}, \tag{37}$$

where $\sum\!\!\!\!\!\!\int_q$ stands for the integration over scattering states and the summation over bound states. The spectral function $\mathbf{A}(\omega,T)$ can then be calculated using equation (1) and a numerical Fourier transform on an equidistant grid in the time domain. This formulation has the advantage that one can obtain $\mathbf{A}(\omega,T)$ for all times T and not just the large time behaviour. But, the NEGF based method is computationally faster and has a better numerical accuracy. Hence, it is used whenever applicable. Of course, both methods yield the same results in the large-time limit.

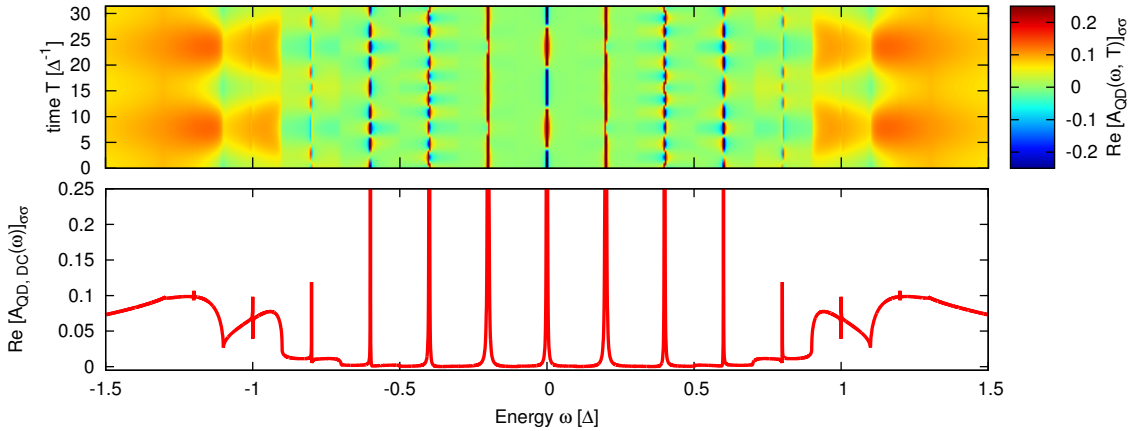

FIG. 3. Top: The spectral function $[\mathbf{A}_{\mathrm{QD}}(\omega,T)]_{\sigma\sigma}$. The results for $\sigma=\uparrow$ and $\sigma=\downarrow$ are identical. Bottom: The time-averaged spectral function $[\mathbf{A}_{\mathrm{QD,DC}}(\omega)]_{\sigma\sigma}$. The bias has been switched on in the past. The imaginary part of the spectral function vanishes. The peaks have a finite width and height. The parameters are: $\Gamma_\alpha=0.5\Delta$ and $U_{\mathrm{L}}=-U_{\mathrm{R}}=0.1\Delta, \eta=10^{-9}\Delta, m_{\max}=20$.

IV. RESULTS - OCCURRENCE OF NEGATIVE VALUES

A. Spectral Function for a constant bias

We start with the presentation of an example demonstrating that a simple probability interpretation of the spectral function is not possible. Figure 3 shows the calculated diagonal elements of the spectral function $\mathbf{A}_{\mathrm{QD}}(\omega,T)$ as well as its time average. Both are computed with the help of the NEGF based method. The bias has been applied in the past. The whole structure is periodic in time according to the Josephson effect with frequency $\omega_{\mathrm{J}}=\frac{2eU}{\hbar}$. Both edges of the superconducting gap structure are split up. The new ones are located at $\Delta\pm\frac{U}{2}$ and $-\Delta\pm\frac{U}{2}$.

Inside the gap, there is a peak structure with a spacing between the peaks of the bias U. In the plot of the time resolved spectral function $\mathbf{A}_{\mathrm{QD}}(\omega,T)$, we further observe small areas with negative values, mostly inside the gap. These findings contradict the interpretation as a time-dependent density of states, which has to be non-negative. The effect is absent in the time-averaged spectral function $\mathbf{A}_{\mathrm{QD,DC}}(\omega)$: It is non-negative for all energies ω. This phenomenon has already been found in a study on metallic rings,[39] but was not further investigated. To the best of our knowledge, negative values of $\mathbf{A}(\omega,T)$ did not occur in all other studies of this quantity.

We investigate this issue and provide a reasonable explanation incorporating these negative areas. The diagonal of the spectral function $\mathbf{A}(\omega,T)$ is an analogue of the Wigner function. The latter is defined as[40]

$$P(x,p)=\frac{1}{2\pi\hbar}\int_{-\infty}^{\infty}dy e^{-ipy/\hbar}\psi\left(x+\frac{y}{2}\right)\left[\psi\left(x-\frac{y}{2}\right)\right]^{\star} \tag{38}$$

$$=\frac{1}{2\pi\hbar}\int_{-\infty}^{\infty}dq e^{iqx/\hbar}\psi\left(p+\frac{q}{2}\right)\left[\psi\left(p-\frac{q}{2}\right)\right]^{\star}. \tag{39}$$

It links the quantum mechanical wave functions $\psi(x)$ and $\psi(p)$ to a phase space distribution $P(x,p)$. But, $P(x,p)$ can have small negative areas.[41] Hence, the simple probability interpretation of the Wigner function $P(x,p)$ is not possible. In fact, it is not unusual that $P(x,p)$ has negative areas. This issue has been solved[42] by taking into account the uncertainty principle:

$$\sigma_x\sigma_p\geq\frac{\hbar}{2}, \tag{40}$$

$$\sigma_x=\sqrt{\langle\hat{x}^2\rangle-\langle\hat{x}\rangle^2}, \tag{41}$$

$$\sigma_p=\sqrt{\langle\hat{p}^2\rangle-\langle\hat{p}\rangle^2}. \tag{42}$$

This means that one cannot determine momentum and position with arbitrary precision at the same time and hence, a phase space distribution $P(x,p)$ with arbitrary sharp values of x and p does not make sense in the quantum world. In order to achieve a measurable quantity one should take a weighted average of $P(x,p)$ in some region, i.e. one should for instance investigate

$$\widetilde{P}(x,p)=\iint_{-\infty}^{\infty}dx'\,dp'P(x',p')M_{\sigma_x,\sigma_p}(x-x',p-p'), \tag{43}$$

$$M_{\sigma_x,\sigma_p}(x,p)=\frac{\hbar}{2\pi\sigma_x\sigma_p}e^{-\frac{x^2}{2\sigma_x^2}-\frac{p^2}{2\sigma_p^2}} \tag{44}$$

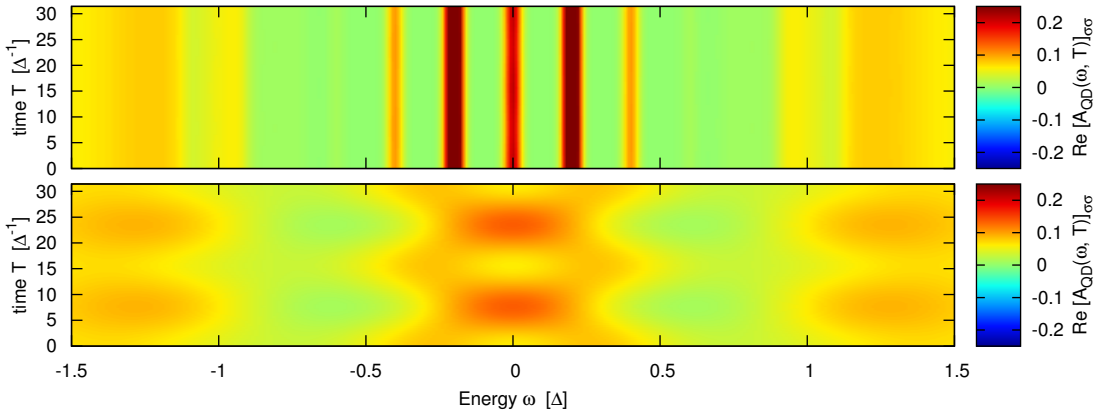

FIG. 4. A plot of the convoluted spectral function $\left[\widetilde{\mathbf{A}}_{\mathrm{QD}}(\omega,T)\right]_{\sigma\sigma}$. It can be compared to the original one $[\mathbf{A}_{\mathrm{QD}}(\omega,T)]_{\sigma\sigma}$ in figure 3 (top). As expected, there are no more negative areas. The standard deviations are: $\sigma_\omega = \frac{1}{50}\Delta$, $\sigma_T = 25\Delta^{-1}$ (top) and $\sigma_\omega = \frac{1}{5}\Delta$, $\sigma_T = \frac{5}{2}\Delta^{-1}$ (bottom). Both examples fulfill $\sigma_\omega\sigma_T = \frac{1}{2}$. All other parameters are identical to those in figure 3.

rather than $P(x,p)$. It has been proven that $\widetilde{P}(x,p)$ is non-negative provided that $\sigma_x, \sigma_p > 0$ and $\sigma_x\sigma_p \geq \frac{\hbar}{2}$.[43] This allows a probability interpretation of $\widetilde{P}(x,p)$ including the momentum and position uncertainties.

B. Recovering the positive semidefiniteness - The convoluted spectral function

The formulation of the spectral function $\mathbf{A}(\omega,T)$ stated in equation (37) is very similar to the Wigner function $P(x,p)$. The time T is the analogue of the momentum p and the frequency ω corresponds to the position x. Hence it is not surprising to see that the spectral function $\mathbf{A}(\omega,T)$ can have small negative areas. The time-energy uncertainty relation plays the same role for $\mathbf{A}(\omega,T)$ as does the x-p uncertainty relation for $P(x,p)$. Like for the Wigner function, we can verify the non-negativity of the convoluted spectral function:

$$0 \leq \left[\widetilde{\mathbf{A}}_{\mathrm{QD}}(\omega,T)\right]_{\sigma\sigma} \tag{45}$$

$$= \iint_{-\infty}^{\infty} d\omega'\, dT' \left[\mathbf{A}_{\mathrm{QD}}(\omega',T')\right]_{\sigma\sigma} \cdot M_{\sigma_\omega,\sigma_T}(\omega-\omega', T-T'), \tag{46}$$

with

$$M_{\sigma_\omega,\sigma_T}(\omega,T) = \frac{1}{2\pi\sigma_\omega\sigma_T} e^{-\frac{\omega^2}{2\sigma_\omega^2} - \frac{T^2}{2\sigma_T^2}}, \tag{47}$$

provided that $\sigma_\omega, \sigma_T > 0$ and $\sigma_\omega\sigma_T \geq \frac{1}{2}$. The proof is carried out in the appendix A.

We further point out that $\mathbf{A}_{\mathrm{QD}}(\omega,T)$ and $\widetilde{\mathbf{A}}_{\mathrm{QD}}(\omega,T)$ are normalized such that

$$1 = \int_{-\infty}^{\infty} d\omega \left[\mathbf{A}_{\mathrm{QD}}(\omega,T)\right]_{\sigma\sigma} \tag{48}$$

$$= \int_{-\infty}^{\infty} d\omega \left[\widetilde{\mathbf{A}}_{\mathrm{QD}}(\omega,T)\right]_{\sigma\sigma} \tag{49}$$

for $\sigma \in \{\uparrow,\downarrow\}$ and all times T. Hence we conclude that $\widetilde{\mathbf{A}}_{\mathrm{QD}}(\omega,T)$ is a probability density function with respect to ω and allows a direct interpretation as a T-dependent density of states. We note in passing that a probability interpretation referring to the variable T is generally not possible because there is no normalization condition with respect to T.

Two different convolutions of the example in figure 3 are shown in figure 4. There are no more negative areas as expected. Hence, the spectral function $\mathbf{A}(\omega,T)$ has to be viewed as a quasiprobability density function and only the convoluted spectral function $\widetilde{\mathbf{A}}_{\mathrm{QD}}(\omega,T)$ should be used for direct comparisons with experiments. Furthermore, the two examples show that it is impossible to resolve the peak structure inside the gap and observe the periodicity due to the Josephson effect simultaneously. The spacing of the peak structure is U and time periodicity is $\frac{\hbar}{e}\frac{\pi}{U}$. Hence, one can not resolve both features simultaneously without violating the time-energy uncertainty relation.

Having this interpretation at hand, we are able to explain the structure inside the gap. It is created by particles that cross the gap with the help of Andreev reflections. This charge transfer mechanism has been used to explain the subharmonic gap structure in several works.[44,45] The negative areas can be viewed as interference effects and reveal the quantum nature of the particles involved.

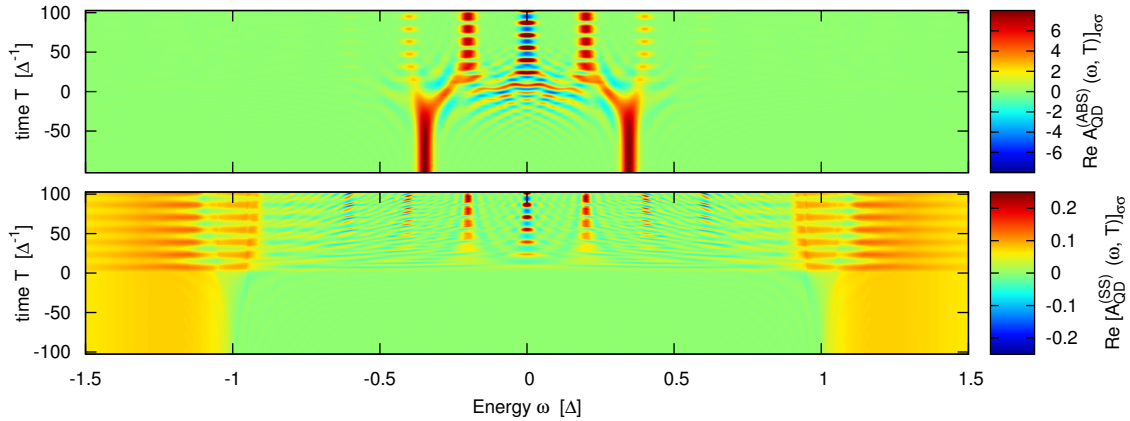

FIG. 5. Decomposition of the full spectral function $\mathbf{A}_{\mathrm{QD}}(\omega, T)$ into contributions of the Andreev bound states $\mathbf{A}_{\mathrm{QD}}^{(\mathrm{ABS})}(\omega, T)$ (top, convoluted in frequency space) and the scattering states $\mathbf{A}_{\mathrm{QD}}^{(\mathrm{SS})}(\omega, T)$ (bottom). The bias is switched on at $t = 0$. The parameters are: $\Gamma_\alpha = 0.5\Delta, U_{\mathrm{L}}(t) = -U_{\mathrm{R}}(t) = 0.1\Delta^{-1}\Theta(t)$.

V. RESULTS - VISUALIZATION OF SWITCHING PROCESSES

We can also visualize switching effects with the help of the spectral function. We prepare the system in the ground state for $t < 0$ and switch on the bias at $t = 0$. The spectral function is split up into contributions of Andreev bound states (labeled $\mathbf{A}_{\mathrm{QD}}^{(\mathrm{ABS})}(\omega, T)$) and scattering states (labeled $\mathbf{A}_{\mathrm{QD}}^{(\mathrm{SS})}(\omega, T)$). All results of this subsection are calculated using the formulation of equation (37) for the spectral function. The Fourier transform with respect to $t - t'$ is done on a grid. We therefore demand for $\mathbf{A}(t, t') \to 0$ as $|t - t'| \to \infty$.

A. Handling bound states

In contrast to the previous results, we now have to take Andreev bound states into account. These underline the importance of the previously discussed convolutions in a second way.

Consider a system with a single bound state (BS) whose energy $\epsilon_{\mathrm{BS}}(t)$ changes adiabatically. Its spectral function $\mathbf{A}^{(\mathrm{BS})}(t, t')$ is then proportional to

$$\mathbf{A}^{(\mathrm{BS})}(t, t') = \psi^{(\mathrm{BS})}(t) \left[\psi^{(\mathrm{BS})}(t')\right]^\star \tag{50}$$

$$\sim e^{+i\epsilon_{\mathrm{BS}}(t)t} e^{-i\epsilon_{\mathrm{BS}}(t')t'}. \tag{51}$$

Hence we can conclude $\mathbf{A}^{(\mathrm{BS})}(t, t') \not\to 0$ as $|t - t'| \to \infty$. If we then calculate the Fourier transform of $\mathbf{A}^{(\mathrm{BS})}(t, t')$ with respect to $\tau = t - t'$, the full past and future relative to the time $T = \frac{t+t'}{2}$ influences the value of $\mathbf{A}^{(\mathrm{BS})}(\omega, T)$. The spectral function $\mathbf{A}^{(\mathrm{BS})}(\omega, T)$ is not just a single peak at $\epsilon_{\mathrm{BS}}(T)$ as one would expect since everything changes adiabatically.

This is in contrast to the most common situation where $\mathbf{A}(t, t') \to 0$ as $|t - t'| \to \infty$. In this case, only the wave functions at times in a neighborhood of $T = \frac{t+t'}{2}$ have an influence on the value of $\mathbf{A}(\omega, T)$. Besides, this allows us to calculate the Fourier transform numerically on a grid.

The most natural way to recover the desired behaviour even in the presence of bound states is to enforce the decay $\mathbf{A}(t, t') \to 0$ as $|t - t'| \to \infty$ by hand. In this way, one mimics a finite lifetime of the bound states. We now show that this is automatically done by the convolution in frequency space presented above.

Using the convolution theorem, the convolution in frequency space can be reformulated as:

$$\frac{1}{\sqrt{2\pi}\sigma_\omega} \int_{-\infty}^{\infty} d\omega' \mathbf{A}(\omega', T) e^{-\frac{(\omega-\omega')^2}{2\sigma_\omega}} = \int_{-\infty}^{\infty} d\tau e^{i\omega\tau} e^{-\frac{\sigma_\omega^2}{2}\tau^2} \mathbf{A}\left(T + \frac{\tau}{2}, T - \frac{\tau}{2}\right). \tag{52}$$

Hence, the convolution of the spectral function adds the desired decay $e^{-\frac{\sigma_\omega^2}{2}(t-t')^2}\mathbf{A}(t, t') \to 0$ as $|t-t'| \to \infty$ even for bound states. Simultaneously, it broadens all sharp frequency peaks of $\mathbf{A}(\omega, T)$.

Since the convolutions smoothen the plots, we only apply it in frequency space to all calculations covering Andreev bound states. The time convolution is not performed in any of the following plots in order to obtain sharper structures. The value of σ_ω is set to $\sqrt{2} \cdot 0.025\Delta$ for all plots covering bound states in this section.

B. Switching on the bias

Figure 5 shows an example of a switching process. The top part shows the contribution of the Andreev bound states $\mathbf{A}_{\mathrm{QD}}^{(\mathrm{ABS})}(\omega, T)$ to the spectral function, the lower part the one of the scattering states $\mathbf{A}_{\mathrm{QD}}^{(\mathrm{SS})}(\omega, T)$. The bias is turned on at $t = 0$.

In the lower part of figure 5, the structure already observed in figure 3 (top) starts to develop after the bias is switched on at $t = 0$. Simultaneously, the Andreev bound states move gradually into the leads. This can hardly be seen in the top figure since the decay rate in the chosen example is too slow compared to the plotted time range. Their contribution to the spectral function will eventually be gone.

We observe effects of the bias already at times $t < 0$ which hints at a violation of causality of the spectral function. But, in order to compare the results with an experiment, one has to apply convolutions as explained above. This resolves the issue for the examples investigated here. Whether this is generally true is currently unknown.

C. Andreev bound states under the influence of a bias pulse

The reformation of the Andreev bound states after a bias pulse is shown in figure 6. Their energy after the bias depends on the accumulated phase $\chi(t) = \frac{2e}{\hbar}\int_0^t dt' U(t')$. In this situation, the location of the Andreev bound states as a function of the phase difference χ can be calculated by solving[38]

$$0 = x^2\left(1 + \frac{\gamma}{\sqrt{1-x^2}}\right) - \frac{\gamma^2}{1-x^2}\frac{1+\cos\chi}{2} \tag{53}$$

with $x = \frac{\omega}{\Delta}$ and $\gamma = \frac{\Gamma}{\Delta}$.

After the pulse, the system does not evolve towards the ground state again, but shows non-decaying oscillations. The frequency is the energy difference of the newly formed Andreev bound states.[38]

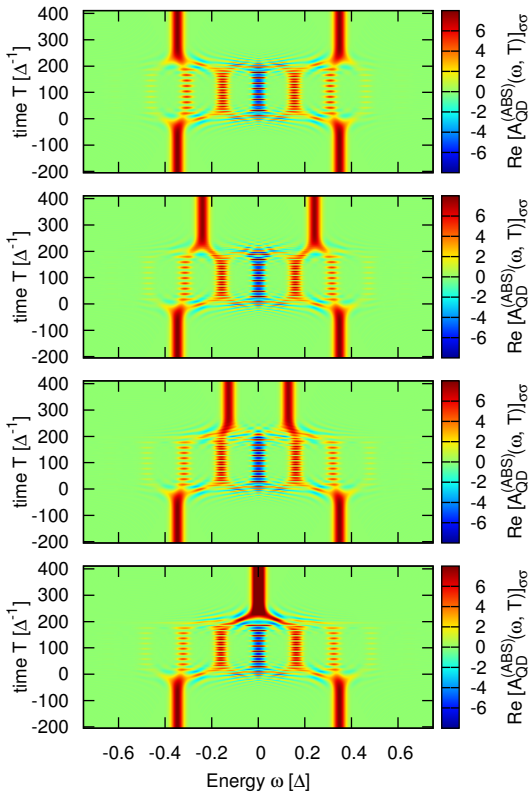

FIG. 6. The spectral function of the Andreev bound states under the influence of a bias pulse from t_0 to t_1. The pulse is chosen such that the accumulated phase is $\Delta\chi = \frac{2e}{\hbar}\int_{t_0}^{t_1} U(t')\,dt' = (20 + x)\pi, x \in \{0, 0.5, 0.75, 1\}$ (from top to bottom), $t_0 = 0, t_1 = 204.8\Delta^{-1}$. The coupling is $\Gamma_\alpha = 0.5\Delta$. The plots show results convoulted in frequency space with $\sigma_\omega = \sqrt{2}\cdot 0.025\Delta$.

VI. CONCLUSIONS

In this paper we have investigated the spectral function $\mathbf{A}(\omega, T)$ for a Josephson junction in the presence of a bias. It turns out that this quantity can occasionally have negative values implying that the interpretation as a time-dependent density of states is problematic. Viewing the spectral function $\mathbf{A}(\omega, T)$ as the time-energy analogue of the Wigner function $P(x, p)$ provides a way out. The latter is well known to have negative values. This issue is solved by looking at averages which then are strictly non-negative. We do the same for the spectral function, which then allows a physically meaningful interpretation as a time-dependent density of states. It provides useful insights into the internal changes of the quantum dot, which are illustrated by three examples differing in the way the bias is turned on: First, the bias is switched on in the past and one looks at the asymptotic behaviour for large times. Second, we look at the transients when switching the bias in a step-like fashion. Third, the reformation of Andreev bound states is shown under the influence of a bias pulse. All three examples show a non-trivial time-dependence which can be nicely understood by interpreting the spectral function $\mathbf{A}(\omega, T)$ as a time-dependent density of states.

Appendix A: Proof

The goal of this section is to prove the following relation:

$$0 \leq \left[\widetilde{\mathbf{A}}_{\mathrm{QD}}(\omega,T)\right]_{\sigma\sigma} \tag{A1}$$

$$= \iint_{-\infty}^{\infty} d\omega'\, dT' \left[\mathbf{A}_{\mathrm{QD}}(\omega',T')\right]_{\sigma\sigma} \cdot M_{\sigma_\omega,\sigma_T}(\omega-\omega',T-T'), \tag{A2}$$

for $\sigma_\omega, \sigma_T > 0$, $\sigma_\omega\sigma_T \geq \frac{1}{2}$ and the Gaussian kernel $M_{\sigma_\omega,\sigma_T}(\omega,T)$ defined as

$$M_{\sigma_\omega,\sigma_T}(\omega,T) = \frac{1}{2\pi\sigma_\omega\sigma_T} e^{-\frac{T^2}{2\sigma_T^2}-\frac{\omega^2}{2\sigma_\omega^2}}. \tag{A3}$$

The proof follows a previous work of Cartwright.[43] We will make use of the subsequent relations:

$$\frac{1}{\sigma\sqrt{2\pi}} \int_{-\infty}^{\infty} dx e^{-\frac{1}{2}\left(\frac{x-\mu}{\sigma}\right)^2} = 1, \tag{A4}$$

$$\frac{1}{\sigma\sqrt{2\pi}} \int_{-\infty}^{\infty} dx e^{i\omega x} e^{-\frac{1}{2}\left(\frac{x-\mu}{\sigma}\right)^2} = e^{-\frac{\sigma^2\omega^2}{2}+i\mu\omega}. \tag{A5}$$

We furthermore define

$$f_{\sigma_\omega,\sigma_T}(x,\omega,T) = \frac{1}{\sqrt{2\pi}} e^{\frac{i\omega}{2}x-\frac{\sigma_\omega^2 x^2}{2}-\frac{x^2-Tx}{2\sigma_T^2}}. \tag{A6}$$

The proof is carried out for $\left[\widetilde{\mathbf{A}}_{\mathrm{QD}}(\omega,T)\right]_{\uparrow\uparrow}$, its generalization for the component $\downarrow$ as well as for other site positions of the tight binding chain is straightforward.

$$\left[\widetilde{\mathbf{A}}_{\mathrm{QD}}(\omega,T)\right]_{\uparrow\uparrow} = \iint_{-\infty}^{\infty} d\omega'\, dT' \left[\mathbf{A}_{\mathrm{QD}}(\omega',T')\right]_{\sigma\sigma} M_{\sigma_\omega,\sigma_T}(\omega-\omega',T-T') \tag{A7}$$

$$= \frac{1}{4\pi^2\sigma_\omega\sigma_T} \iiint_{-\infty}^{\infty} d\omega'\, dT'\, d\tau' \left[\mathbf{A}_{\mathrm{QD}}\left(T'+\frac{\tau'}{2}, T'-\frac{\tau'}{2}\right)\right]_{\uparrow\uparrow} e^{i\omega'\tau'} e^{-\frac{(T-T')^2}{2\sigma_T^2}-\frac{(\omega-\omega')^2}{2\sigma_\omega^2}} \tag{A8}$$

$$= \frac{\sqrt{2\pi}}{4\pi^2\sigma_T} \iint_{-\infty}^{\infty} dT'\, d\tau' \left[\mathbf{A}_{\mathrm{QD}}\left(T'+\frac{\tau'}{2}, T'-\frac{\tau'}{2}\right)\right]_{\uparrow\uparrow} e^{-\frac{\sigma_\omega^2\tau'^2}{2}+i\tau'\omega} e^{-\frac{(T-T')^2}{2\sigma_T^2}} \tag{A9}$$

$$\underset{y=T'-\frac{\tau'}{2}}{\overset{x=T'+\frac{\tau'}{2}}{=}} \frac{2}{2\pi\sqrt{2\pi}\sigma_T} \iint_{-\infty}^{\infty} dx\, dy \left[\mathbf{A}_{\mathrm{QD}}(x,y)\right]_{\uparrow\uparrow} e^{-\frac{\sigma_\omega^2(x-y)^2}{2}+i(x-y)\omega} e^{-\frac{(T-\frac{x+y}{2})^2}{2\sigma_T^2}} \tag{A10}$$

$$= \frac{2e^{-\frac{T^2}{2\sigma_T^2}}}{\sqrt{2\pi}\sigma_T} \iint_{-\infty}^{\infty} dx\, dy \sum\!\!\!\!\!\!\int_q u_{q,\mathrm{QD}}(x) \left[u_{q,\mathrm{QD}}(x)\right]^\star f(x,\omega,T) \left[f(y,\omega,T)\right]^\star e^{\sigma_\omega^2 xy-\frac{xy}{4\sigma_T^2}} \tag{A11}$$

$$= \underbrace{\frac{2e^{-\frac{T^2}{2\sigma_T^2}}}{\sqrt{2\pi}\sigma_T}}_{>0,\ \text{since } \sigma_T>0} \sum\!\!\!\!\!\!\int_q \sum_{k=0}^{\infty} \underbrace{\frac{(\sigma_\omega^2-\frac{1}{4\sigma_T^2})^k}{k!}}_{\geq 0,\ \text{since } \sigma_\omega\sigma_T\geq\frac{1}{2}} \tag{A12}$$

$$\underbrace{\left[\int_{-\infty}^{\infty} dx\ u_{q,\mathrm{QD}}(x) f(x,\omega,T) x^k\right] \left[\int_{-\infty}^{\infty} dy\ u_{q,\mathrm{QD}}(y) f(y,\omega,T) y^k\right]^\star}_{=CC^\star=|C|^2\geq 0}$$

$$\geq 0. \tag{A13}$$

[1] A. Aviram and M. A. Ratner, Chemical Physics Letters **29**, 277 (1974).

[2] G. Cuniberti, G. Fagas, and K. Richter, *Introducing Molecular Electronics* (Springer, 2005).

[3] M. Di Ventra, *Electrical Transport in Nanoscale Systems*, 1st ed. (Cambridge University Press, 2008).

[4] J. C. Cuevas and E. Scheer, *Molecular Electronics* (World Scientific Publishing Company, 2010).

[5] P. Myöhänen, A. Stan, G. Stefanucci, and R. van Leeuwen, Physical Review B **80**, 115107+ (2009).

[6] P. Myöhänen, A. Stan, G. Stefanucci, and R. van Leeuwen, Journal of Physics: Conference Series **220**, 012017+ (2010).

[7] A. M. Uimonen, E. Khosravi, G. Stefanucci, S. Kurth, R. van Leeuwen, and E. K. U. Gross, Journal of Physics: Conference Series **220**, 012018+ (2010).

[8] A. M. Uimonen, E. Khosravi, A. Stan, G. Stefanucci, S. Kurth, R. van Leeuwen, and E. K. U. Gross, Physical Review B **84**, 115103+ (2011).

[9] E. Khosravi, A. M. Uimonen, A. Stan, G. Stefanucci, S. Kurth, R. van Leeuwen, and E. K. U. Gross, Physical Review B **85**, 075103+ (2012).

[10] G. Stefanucci and R. van Leeuwen, *Nonequilibrium Many-Body Theory of Quantum Systems: A Modern Introduction* (Cambridge University Press, 2013).

[11] M. Knap, W. von der Linden, and E. Arrigoni, Physical Review B **84**, 115145+ (2011).

[12] E. Runge and E. K. U. Gross, Physical Review Letters **52**, 997 (1984).

[13] R. Baer, T. Seideman, S. Ilani, and D. Neuhauser, The Journal of chemical physics **120**, 3387 (2004).

[14] K. Burke, R. Car, and R. Gebauer, Physical Review Letters **94**, 146803+ (2005).

[15] S. Kurth, G. Stefanucci, C. O. Almbladh, A. Rubio, and E. K. U. Gross, Physical Review B **72**, 035308+ (2005).

[16] J. Yuen-Zhou, C. Rodriguez-Rosario, and A. Aspuru-Guzik, Phys. Chem. Chem. Phys. **11**, 4509 (2009).

[17] M. Di Ventra and R. D'Agosta, Physical Review Letters **98**, 226403+ (2007).

[18] H. Appel and M. Di Ventra, Physical Review B **80**, 212303+ (2009).

[19] H. Appel and M. Di Ventra, Chemical Physics **391**, 27 (2011).

[20] Y. Wang, C. Y. Yam, T. Frauenheim, G. H. Chen, and T. A. Niehaus, Chemical Physics **391**, 69 (2011).

[21] Y. Zhang, S. Chen, and G. H. Chen, Physical Review B **87**, 085110+ (2013).

[22] C. Oppenländer, B. Korff, T. Frauenheim, and T. A. Niehaus, Phys. Status Solidi B **250**, 2349 (2013).

[23] J. Jin, X. Zheng, and Y. Yan, The Journal of Chemical Physics **128**, 234703+ (2008).

[24] X. Zheng, J. Jin, and Y. Yan, New Journal of Physics **10**, 093016+ (2008).

[25] X. Zheng, J. Jin, and Y. Yan, The Journal of Chemical Physics **129**, 184112+ (2008).

[26] J. Zanghellini, M. Kitzler, T. Brabec, and A. Scrinzi, Journal of Physics B: Atomic, Molecular and Optical Physics **37**, 763+ (2004).

[27] H. Wang and M. Thoss, The Journal of Chemical Physics **131**, 024114+ (2009).

[28] H. Wang and M. Thoss, J. Phys. Chem. A **117**, 7431 (2013).

[29] K. F. Albrecht, H. Wang, L. Mühlbacher, M. Thoss, and A. Komnik, Physical Review B **86**, 081412+ (2012).

[30] L. Mühlbacher and E. Rabani, Physical Review Letters **100**, 176403+ (2008).

[31] T. Burnus, M. A. L. Marques, and E. K. U. Gross, Physical Review A **71**, 010501+ (2005).

[32] E. Räsänen, A. Castro, and E. K. U. Gross, Physical Review B **77**, 115108+ (2008).

[33] R. Peierls, *Zeitschrift für Physik*, Zeitschrift für Physik A Hadrons and Nuclei **80**, 763 (1933).

[34] Y. Nambu, Physical Review Online Archive (Prola) **117**, 648 (1960).

[35] G. Stefanucci, S. Kurth, E. K. U. Gross, and A. Rubio, "Time-dependent transport phenomena," (Elsevier, 2007) Chap. 10, pp. 247–284.

[36] G. Stefanucci, S. Kurth, A. Rubio, and E. K. U. Gross, Physical Review B **77**, 075339+ (2008).

[37] E. Perfetto, G. Stefanucci, and M. Cini, Physical Review B **80**, 205408+ (2009).

[38] G. Stefanucci, E. Perfetto, and M. Cini, Physical Review B **81**, 115446+ (2010).

[39] L. Arrachea, Physical Review B **66**, 045315+ (2002).

[40] E. Wigner, Physical Review **40**, 749 (1932).

[41] W. Schleich, *Quantum optics in phase space* (Wiley-VCH, 2001).

[42] S. Stenholm, European Journal of Physics **1**, 244+ (1980).

[43] N. D. Cartwright, Physica A: Statistical Mechanics and its Applications **83**, 210 (1975).

[44] A. Levy Yeyati, J. C. Cuevas, A. López-Dávalos, and A. Martín-Rodero, Physical Review B **55**, R6137 (1997).

[45] G. Johansson, E. N. Bratus, V. S. Shumeiko, and G. Wendin, Physical Review B **60**, 1382 (1999).